Current Applied Physics 14 (2014) 659–664

Contents lists available at ScienceDirect

Current Applied Physics

journal homepage: www.elsevier.com/locate/cap

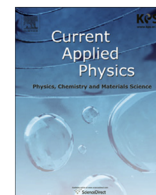

# Dark current suppression of amorphous selenium based photosensors by the ZnO hole blocking layer

Tung-Yuan Yu [a], Fu-Ming Pan [a,*], Cheng-Yi Chang [a], Tien Hu [a], Jenn-Fang Chen [b], Jia-Feng Wang [b], Cheng-Lu Lin [b], Tsung-Han Chen [c], Te-Ming Chen [c]

[a] *Department of Materials Science and Engineering, National Chiao-Tung University, 1001 Ta Hsueh Road, Hsinchu 30010, Taiwan, ROC*
[b] *Department of Electrophysics, National Chiao-Tung University, Hsinchu 30010, Taiwan, ROC*
[c] *AU Optronics Corporation, Hsinchu Science Park, Hsinchu 30078, Taiwan, ROC*

ARTICLE INFO

*Article history:*
Received 26 November 2013
Received in revised form
7 February 2014
Accepted 13 February 2014
Available online 4 March 2014

*Keywords:*
Zinc oxide
Amorphous Se
Hole blocking layer
Oxygen vacancy
DLTS

ABSTRACT

To study the influence of defects in the hole blocking layer (HBL) on the dark current of amorphous selenium (a-Se) based photosensors, we prepared ZnO thin films by reactive sputter deposition (RSD) for the use as the HBL of the photosensors. The ZnO HBL layers prepared with different oxygen flow rates were characterized by X-ray photoelectron spectroscopy, Raman scattering analysis and photoluminescence, indicating that the density of oxygen vacancies in the ZnO thin films is significantly affected by the oxygen flow rate. The deep level transient spectroscopy measurement reveals two hole trap levels present in the RSD deposited ZnO thin films; one is at 0.94 eV and the other at 0.24 eV above the valence band edge. The electrical performance of the a-Se photosensor is largely influenced by the amount of oxygen vacancies in the ZnO thin film. The a-Se photosensor with the ZnO HBL of the most oxygen vacancies has the lowest dark current and demonstrates the highest breakdown field.

© 2014 Elsevier B.V. All rights reserved.

## 1. Introduction

Zinc oxide is a direct wide band gap oxide semiconductor with the band gap in the near ultraviolet (UV) spectral region and a large exciton binding energy of 60 meV [1–3]. As-grown ZnO is usually an n-type semiconductor because of the presence of intrinsic defects that introduce donor levels in the band gap, such as interstitial zinc and oxygen vacancies. Owing to many advantageous material and optoelectronic properties, ZnO has received extensive research on chemical and optoelectronic applications in the past few decades, such as transparent thin-film transistors, photosensors, blue/UV light-emitting diodes and chemical sensors. Among the wide variety of promising applications, the use of ZnO as the hole blocking layer (HBL) for organic photovoltaic devices has been proposed based on its n-type nature with the wide band gap [4–6]. In this study, we used ZnO thin films as the HBL for amorphous selenium (a-Se) based photosensors, which have recently received much attention for X-ray imaging applications [7–9].

The photoconversion quantum efficiency of a-Se is drastically increased when the electric bias reaches a field of >70 V/μm. This effect is due to the avalanche multiplication of impact ionization kindled by hole carriers drifting at the high electric field [10,11]. The avalanche effect makes a-Se a prominent photoconductors for imaging applications that require operations under an illumination condition of very low photon dose, such as medical X-ray imaging [7,12,13]. However, the high photoconversion gain at the high field is usually accompanied by a high dark current, resulting in the degradation in the image contrast. The dark current is mainly contributed from the hole injection from the anode to the a-Se active layer [14,15]. In order to suppress the dark current, a-Se based photoconductors require an HBL to impede the hole injection. In contemporary a-Se photosensors, such as high-gain avalanche rushing photoconductor (HARP), the HBL is generally made of a $CeO_2$ thin film. Based on the observation of time dependence of the dark current at different bias fields, the hole blocking mechanism is generally proposed to be associated with hole trapping in the $CeO_2$ HBL [16–18]. The hole trapping results in charge accumulation in the blocking layer and a potential barrier is thus developed by the positive space charges, thereby suppressing hole carrier injection from the anode. Because the hole trapping is closely related to defects present in the HBL, and ZnO is one of the n-type oxide semiconductors that have been extensively studied on the nature of defects, we used ZnO thin films as the HBL layer of a-Se photosensors in this study. Fig. 1 shows the interface band

* Corresponding author. Tel.: +886 3 5131322; fax: +886 3 5724727.
*E-mail address:* fmpan@faculty.nctu.edu.tw (F.-M. Pan).

http://dx.doi.org/10.1016/j.cap.2014.02.011
1567-1739/© 2014 Elsevier B.V. All rights reserved.

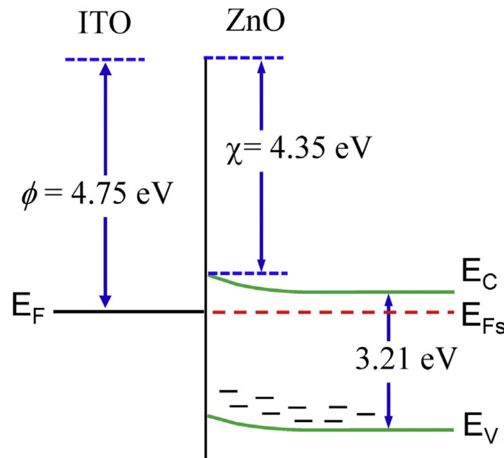


**Fig. 1.** The interface band diagram for the ITO/ZnO heterojunction. $E_F$ and $\phi$ represent the Fermi level and the work function of ITO, respectively. Labels for the ZnO semiconductor are follows: $E_{Fs}$: Fermi level, $\chi$: electron affinity, $E_C$: conduction band edge and $E_V$: valence band edge. Hole trap centers in ZnO are illustrated as the short lines near $E_V$.

diagram of the heterojunction between ZnO and indium doped tin oxide (ITO) to illustrate hole traps in the ZnO layer. The work function of ITO (4.75 eV) and the electron affinity of ZnO (4.35 eV) are collected from the literature [19,20], and the band gap of ZnO is experimentally obtained in the study as discussed later. Hole carriers injected from the ITO electrode can be trapped in deep trap centers in the ZnO HBL. Increasing trap centers in the ZnO HBL is beneficial for lowering the dark current of the photosensors. The properties of intrinsic defects in ZnO highly depend on the growth techniques, growth conditions and post-growth thermal treatment [21,22]. We prepared the ZnO HBL by reactive sputter deposition (RSD), and X-ray photoelectron spectroscopy (XPS), photoluminescence (PL) and Raman scattering spectroscopy were used to study oxygen vacancies present in the ZnO thin films. The measurement of hole trap levels was performed by deep level transient spectroscopy (DLTS).

## 2. Experimental

ZnO thin films were deposited on the ITO glass or the $SiO_2$ substrate at room temperature by reactive sputter deposition in a magnetron sputtering system using a Zn metal target of 99.9% in purity. The ZnO thin film was deposited on the thermally oxidized Si wafer for material characterizations, while, for the fabrication of a-Se photosensors, it was deposited on the ITO glass. During the ZnO film deposition, the argon flow rate was kept at 20 sccm and the oxygen flow rate varied from 10 to 50 sccm; the sputtering power and the working pressure was 50 W and $1 \times 10^{-2}$ torr, respectively. All the ZnO samples prepared with different $O_2$ flow rates at a constant Ar flow rate of 20 sccm had a thickness of 50 nm.

The major carrier concentration of ZnO thin films was analyzed by Hall-effect measurements (Ecopia HMS-3000). The surface morphology of ZnO thin films was examined by scanning electron microscopy (SEM, JEOL JSM-6500F) and atomic force microscope (AFM, Bruker Dimension Icon). The microstructure of the ZnO thin films was analyzed by transmission electron microscopy (TEM, JEOL JEM-3000F) and X-ray diffraction spectroscopy (XRD, Bruker D8 Advance) using the Cu K$\alpha$ source. The incident angle of the X-ray beam with respect to the sample surface is 1° during the XRD analysis. A Horiba Jobin Yvon LABRAM HR800 spectrometer was used to study Raman scattering of the ZnO thin films using an Ar-ion laser as the excitation source. The surface chemical composition of the ZnO thin films was analyzed by X-ray photoelectron spectroscopy (XPS, Thermo VG 350). Photoluminescence (PL) emission at room temperature from the ZnO thin films was studied by a PL spectrometer (Horiba Jobin Yvon iHR-320). DLTS (Sula Technologies) was conducted at the temperature range between 110 and 350 K and at a quiescent bias of 0 V with the filling pulse height of 5 V into the reverse bias and a width of 100 ms. For the DLTS measurement, the ZnO thin film with a thickness of 800 nm was deposited on a 500 nm thick $SiO_2$ layer thermally grown on the Si wafer, and Pd and Al were used as the schottky and ohmic contacts, respectively.

The a-Se photosensor fabricated in the study is basically with the HARP device structure without the electron hole blocking layer. Fig. 2 schematically shows the cross-sectional structure of the a-Se photosensor. We first deposited the 50 nm-thick ZnO HBL on the ITO glass substrate at room temperature, followed by the deposition of an a-Se film of 13 μm in thickness at 30 °C by thermal evaporation deposition. A cellulose acetate (CA) polymer film of 2 μm in thickness was then spin-coated on the a-Se layer before the electron beam deposition of the Al electrode pad with an area of 1 $mm^2$. The CA polymer film was used as a distributed resistive layer (DRL), which can mitigate electrical discharge at electrode edges due to the high electrical stress during photosensing operation [23,24]. The dark current of the a-Se photosensors was measured with a Keithley 237 source-measure unit.

## 3. Results and discussion

Five ZnO thin films were prepared by reactive sputter deposition with different $O_2$ flow rates at a constant Ar flow rate of 20 sccm. We will designate thereafter the ZnO thin films by ZnO-X, where X represents the $O_2$ flow rate in sccm. The electron density of all the ZnO samples measured by Hall-effect is in the order of $10^{13}$ $cm^{-3}$. The ZnO-20 thin film has the highest electron density ($8.53 \times 10^{13}$ $cm^{-3}$) and the ZnO-10 thin film has the smallest one ($2.37 \times 10^{13}$ $cm^{-3}$). Fig. 3(a) and (b) shows the plane-view SEM and AFM images of the ZnO-20 thin film, respectively. The surface of the thin film has a root-mean-square roughness of ~1.64 nm according to the AFM analysis. The variation in the $O_2$ flow rate results in little difference in the surface topography and the microstructure of the ZnO thin films. Fig. 3(c) shows the cross-sectional SEM image of a 50 nm thick ZnO-20 thin film capped by a 13 μm thick a-Se layer,

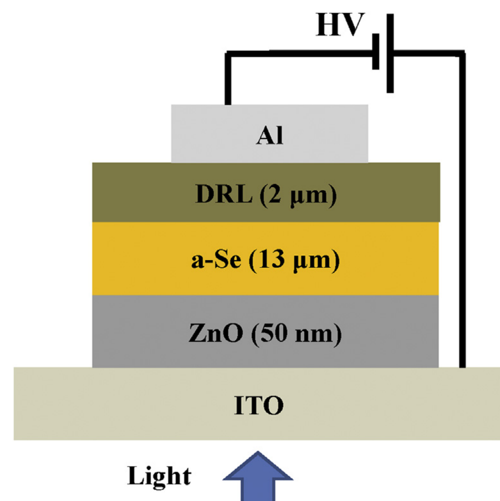


**Fig. 2.** Schematic device structure of the a-Se photosensor with the ZnO HBL.

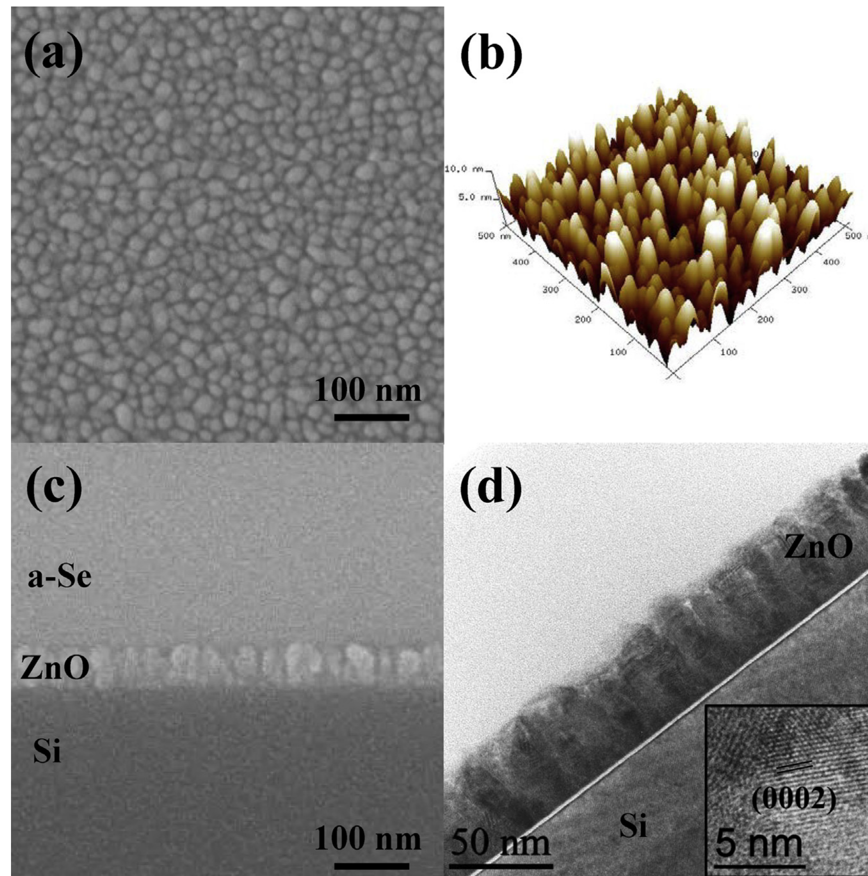


**Fig. 3.** The Plane-view SEM image (a) and the AFM image (b) of the ZnO-20 thin film; (c) cross-sectional SEM image of the ZnO-20 thin film overlaid by a 13 μm thick a-Se layer; (d) the cross-sectional TEM image of the ZnO-20 thin film with the inset showing a high-resolution image.

indicating that the thin film has a microstructure composed of equiaxed and columnar grains with a size in the order of 20–30 nm. The cross-sectional TEM image of the ZnO-20 thin film is shown in Fig. 3(d) with a high resolution image (inset) showing the lattice fringe of the ZnO (0002) plane (~0.26 nm). Fig. 4 shows XRD spectra of ZnO thin films deposited with various oxygen flow rates. The distinct peak at 34.4° corresponds to the (0002) lattice plane of the ZnO hexagonal wurtzite structure, indicating that the ZnO thin

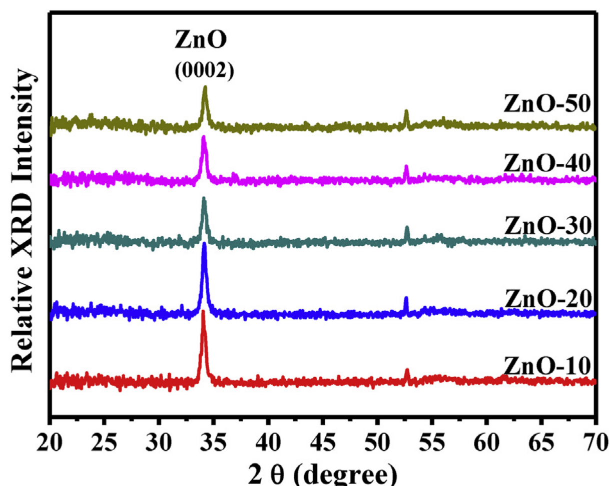


**Fig. 4.** XRD spectra of the ZnO thin films deposited with different $O_2$ flow rates.

films have a preferential orientation in the direction of the c-axis. Because the (0002) plane of wurtzite ZnO has the smallest surface free energy compared with other lattice planes, the sputter-deposited ZnO thin films tend to grow along the c-axis orientation [25]. Based on the Scherrer equation, the average grain size of the ZnO thin films is around 20 nm, which is consistent with the observation of the cross-sectional SEM image.

Fig. 5(a) shows XPS spectra of the O1s electron for the ZnO samples. The O 1s XPS signal can be curve-fitted with three peak components assuming a Gaussian–Lorentzian peak shape [26–29]. The $O_a$ peak at 530.1 eV is due to lattice oxygen ions ($O^{2-}$) in the ZnO wurtzite structure, and the $O_c$ peak at 532.3 eV can be attributed to adsorbed species on the ZnO surface, such as $H_2O$ and weakly adsorbed $O_2$ molecules. The $O_b$ peak at 531.2 eV is generally assigned to $O^-$ ions, which are associated with oxygen vacancies ($V_O$) in the surface layer of the ZnO thin films [26,30]. Fig. 5(b) presents the ratio of the peak area of the individual peaks to the summed area of the three component peaks as a function of the $O_2$ flow rate used for the ZnO deposition. It is obvious from the figure that the $O_b$ peak of the ZnO-20 sample has the largest area ratio, suggesting that the ZnO-20 thin film has the highest oxygen vacancy density. Raman scattering study discussed below supports the observation by XPS.

Fig. 6 shows Raman spectra ranging from 350 $cm^{-1}$ to 650 $cm^{-1}$ for the ZnO thin films. The fluorescence-background has been removed from the Raman spectra. A broad peak is observed in the range between 375 and 475 $cm^{-1}$, which can be assigned to the superposition of three Raman peaks, $A_1$(TO) (380 $cm^{-1}$), $E_1$(TO) (407 $cm^{-1}$) and $E_2$(high) (473 $cm^{-1}$) [31]. The $E_2$(high) mode is

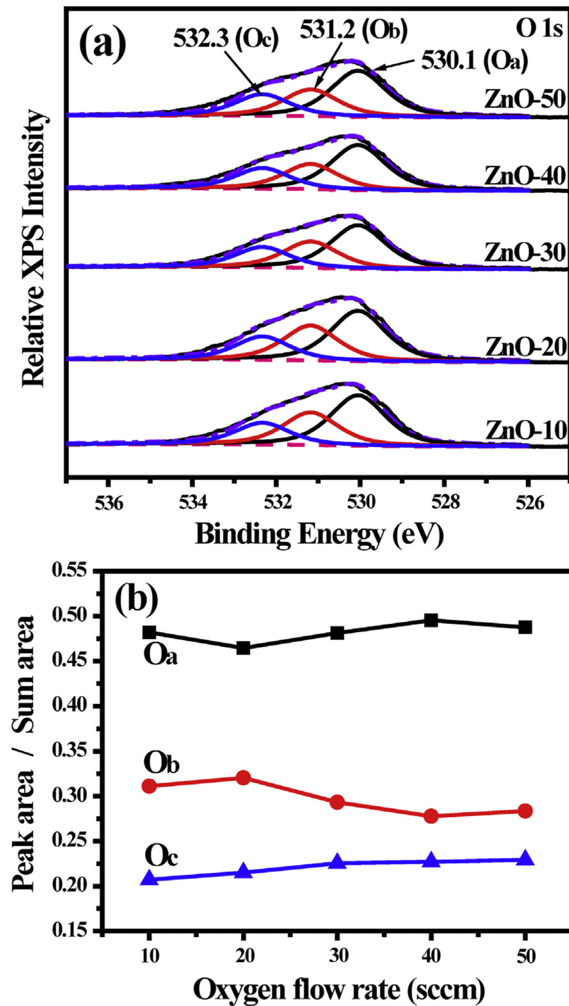


**Fig. 5.** (a) O 1s XPS spectra of the ZnO thin films deposited with various $O_2$ flow rates; (b) the ratio of the peak area of the three component peaks to the summed area as a function of the $O_2$ flow rate.

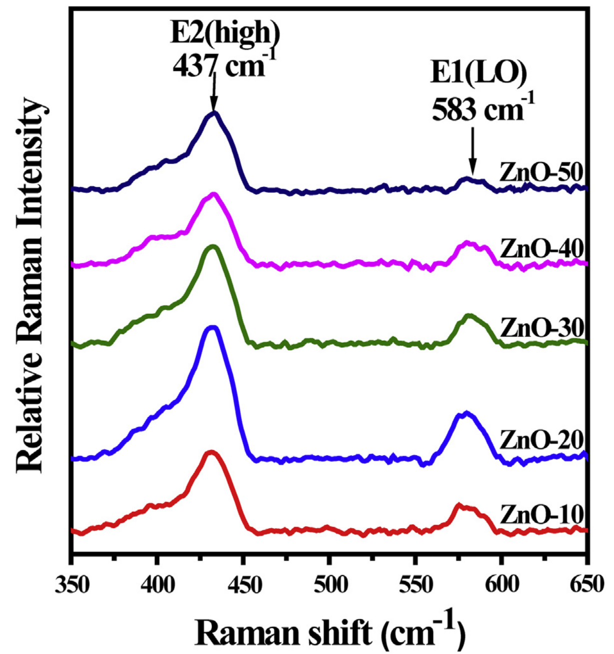


**Fig. 6.** Raman spectra of the ZnO thin films deposited with different $O_2$ flow rates.

associated with oxygen vibration and its frequency shifts if lattice distortion occurs in the ZnO film. According to the Raman spectra, all the ZnO samples have the $E_2$(high) peak situated at 437 cm$^{-1}$, indicating that the variation of the $O_2$ flow rate results in little effect on the lattice strain of the ZnO samples. On the other hand, all samples except the ZnO-20 has the $E_1$(LO) peak centered at 583 cm$^{-1}$. Because the $A_1$(LO) mode, which is situated at 574 cm$^{-1}$ for wurtzite ZnO, is obviously absent in the Raman spectra of all the ZnO samples other than the ZnO-20, we attribute the lower peak position (~4 cm$^{-1}$) of the ZnO-20 thin film to a redshift of the $E_1$(LO) peak but not an interference from the $A_1$(LO) mode. A small redshift of the $E_1$(LO) mode can be ascribed to the presence of point defects, such as O-vacancy and Zn-interstitial, in the ZnO wurtzite lattice [31]. The observed redshift of the $E_1$(LO) mode is in agreement with the XPS study, which shows that the ZnO-20 has a higher concentration of oxygen vacancy than the other ZnO samples. Therefore, we believe that the ZnO-20 thin film has a larger $V_O$ density than other ZnO samples.

The room temperature PL spectra of the ZnO thin films are shown in Fig. 7. The sharp luminescence peak situated at 377 nm is due to the near-band-edge emission. The broad band emission ranging from 450 nm to 700 nm is centered at 550 nm, which is generally attributed to defect-related deep level emissions in the ZnO thin film [32–34]. The peak position and shape of the green band has little dependence on the oxygen flow rate for the ZnO deposition. Therefore, the green band emission of all the ZnO thin films must be induced from the same electronic transition process involving a specific defect level. The relative concentration of the defect centers resulting in the green PL thin film can be estimated by the PL intensity (peak height) ratio of the green emission ($I_{gr}$) to the edge emission ($I_{uv}$). The inset of Fig. 7 shows the $I_{gr}/I_{uv}$ ratio as a function of the oxygen flow rate. The ZnO-20 sample has the largest PL ratio suggesting that it has the highest concentration of the defect producing the green emission. Although the PL emission of ZnO has been extensively studied, the origin of the green band emission is still under much debate. Among the various defects proposed to be responsible for the green PL emission of ZnO, oxygen vacancies are the most often suggested defect inducing the emission, which is considered to result from electron–hole recombination in singly ionized $V_O$ centers situated about 0.9 eV above the valence band maximum (VBM) of ZnO [21,35–39]. Because the XPS and Raman analyses reveal that the ZnO-20 thin film has a larger $V_O$ density than other ZnO samples, the green emission is likely associated with $V_O$ related defect centers. We do find by DLTS analysis that a deep level trap is present at 0.9 eV above the VBM.

Fig. 8(a) presents the DLTS spectrum of the ZnO-20 sample showing two signal dips. The two hole-trap related signals have the minimum at 216 K (L1) and at 287 K (L2). The thermal emission activation energy of the two trap levels can be determined by the Arrhenius plot as shown in Fig. 8(b), in which $\ln(\tau T^2)$ is plotted against $1000/T$, where $\tau$ is the capacitance transient time constant deduced from the DLTS window setting and $T$ is the absolute temperature [40]. The activation energy of the thermal emission of the L1 and L2 traps are thus calculated to be 0.246 eV and 0.942 eV, respectively, with respect to the VBM. The trap density derived from the DLTS measurement is $1.50 \times 10^{11}$ cm$^{-3}$ and $2.93 \times 10^{11}$ cm$^{-3}$ for L1 and L2, respectively. A defect level at ~0.9 eV above VBM has been previously reported in the defect study of ZnO by DLTS [41,42]. Much research, including theoretical and experimental studies, has proposed that the energy level

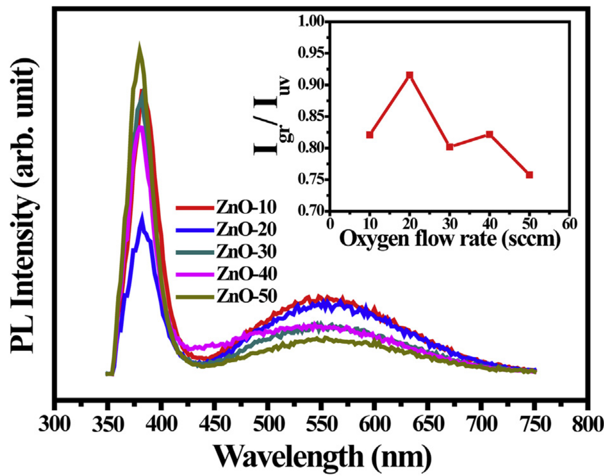


**Fig. 7.** PL spectra of the ZnO thin films deposited with various $O_2$ flow rates. Inset is the peak height ratios of the green band emission to the band edge emission as a function of the $O_2$ flow rate. (For interpretation of the references to color in this figure legend, the reader is referred to the web version of this article.)

around 0.9 eV is due to oxygen vacancies [41,43–46]. The measured activation energy for the L2 hole trap is in very good agreement with the theoretical value obtained by Lany et al. for the $V_O(+/0)$ transition level [44]. The reactive sputter-deposited ZnO thin films have an optical band gap of 3.21 eV as determined by the Tauc plot based on the ultraviolet–visible absorption spectroscopy analysis.

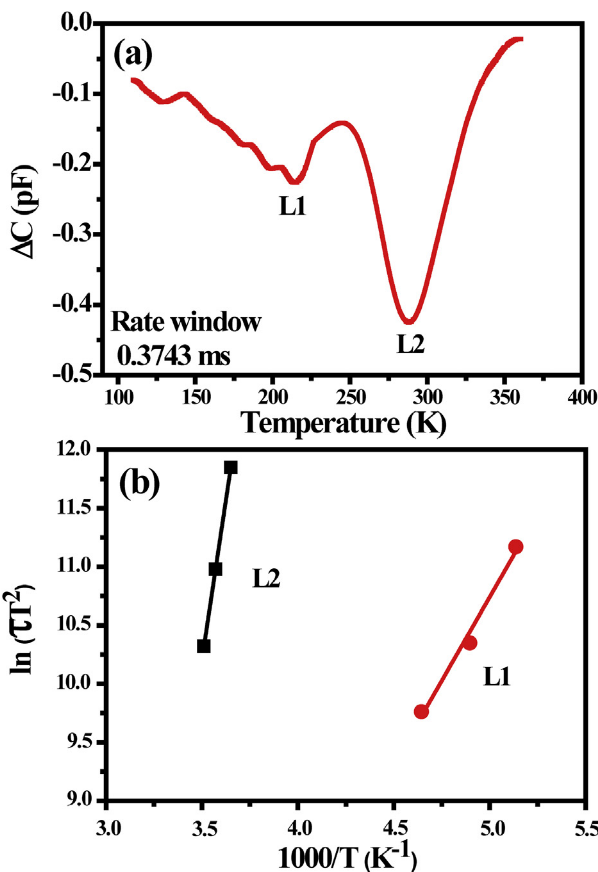


**Fig. 8.** (a) The DLTS spectrum of the ZnO-20 thin film (rate window time constant $\tau$ = 0.3743 ms); (b) the corresponding Arrhenius plots for the hole trap levels measured by DLTS analysis.

If electronic transition from the experimentally determined conduction band minimum to the L2 level takes place, a green band emission can occur at 2.27 eV (~546 nm), which is consistent with the observation in the PL spectra in Fig. 7. The defect identity associated with the L1 level is unclear to us presently. If radiative electronic transition between the conduction band minimum and the L1 level is allowed, it can produce a violet emission at 2.96 eV (~419 nm). However, the violet emission may be obscured by the band edge emission in this study as a result of the small concentration of the L1-related defect. Because the ZnO-20 sample has the largest concentration of $V_O$ as revealed by the PL spectra than the other samples, it is expected to produce the lowest dark current in the a-Se photosensor when used as the HBL.

Fig. 9 shows the dark current density of the a-Se photosensors with the ZnO HBL as a function of the electric field. The dark current density of the a-Se device without the ZnO HBL is about $2 \times 10^{-11}$ A/mm$^2$ at a field of 10 V/μm. When the 50 nm thick ZnO HBL is present in the a-Se photosensor, the dark current density at 10 V/μm is reduced by nearly one order of magnitude for all the devices with different oxygen flow rates. The dark current density increases with the electric field and demonstrates a sudden increase in a certain field range, indicating the breakdown of the device. The device with the ZnO-20 HBL shows the smallest increase rate of the dark current density (~$1 \times 10^{-11}$ A/mm$^2$ at 40 V/μm) and the highest breakdown field (>50 V/μm). The better electrical performance of the ZnO-20 device can be ascribed to a higher concentration of the $V_O$, which may form the deep hole trap center at 0.942 eV as discussed above, and thus has a better suppression effect on hole injection from the ITO anode into the a-Se active layer. It has been reported that more defect levels in the $CeO_2$ HBL of a-Se photosensors will lower the potential barrier for holes between the anode and the HBL, thus leading to an increase in the dark current [47]. However, our result seems to indicate that the variation in the $V_O$ concentration in the ZnO HBLs affects insignificantly the potential barrier height. From Fig. 9, a larger dark current triggers the device breakdown at a lower electric field; this may be a consequence of the local Joule heating effect. Because the a-Se layer was prepared without the addition of any impurity, such as arsenic, it has a very low glass transition temperature (~41 °C according to differential scanning calorimetry analysis). The Joule effect can induce crystallization of the a-Se layer at the low temperature and thereby increases the conductivity of the photoconductor leading to the breakdown [12,48]. The ZnO-20 photoconductor device has the highest breakdown field as a result of the smallest dark current density.

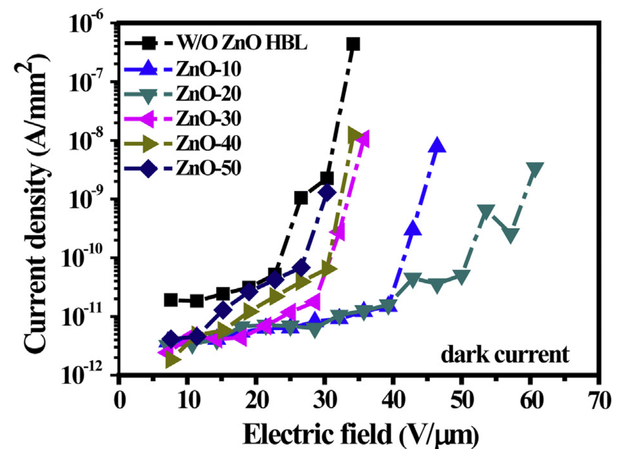


**Fig. 9.** The dark current of the a-Se photoconductors with the HBL prepared using different $O_2$ flow rates as a function of the electric field.

## 4. Conclusion

We prepared ZnO thin films by reactive sputter deposition, and used as the HBL for a-Se based photoconductor devices. The $Ar/O_2$ flow rate ratio used for the ZnO deposition has a significant effect on material and electrical properties of the ZnO HBL. We correlated oxygen vacancies in the ZnO thin film with the dark current suppression capability of the HBL by XPS, Raman, PL and DLTS analyses. The XPS, Raman and PL measurements indicate that the ZnO thin film prepared with the $Ar/O_2$ flow rate ratio of 20 sccm/20 sccm has the highest concentration of oxygen vacancies, which create a hole trap level at 0.94 eV above the valence band edge according to the DLTS measurement. The electronic transition from the conduction band edge to the hole trap level results in the green emission centered at 2.72 eV. The a-Se photosensor with the ZnO-20 HBL has the best photoconduction performance, including the lowest dark current and the highest breakdown field. We believe that oxygen vacancies in the HBL layer play as hole trap centers to suppress the hole injection from the ITO anode of the a-Se photosensor as proposed by many previous reports.

## Acknowledgments

We thank the National Science Council of R.O.C. and AU Optronics Corporation for the financial support. The technical support of the National Nano Device Laboratories is also gratefully acknowledged.

## References

[1] A. Janotti, C. G. V. d. Walle, Rep. Prog. Phys. 72 (2009) 126501.
[2] Ü. Özgür, Y.I. Alivov, C. Liu, A. Teke, M.A. Reshchikov, S. Doğan, V. Avrutin, S.-J. Cho, H. Morkoç, J. Appl. Phys. 98 (2005) 041301.
[3] G.W. Tomlins, J.L. Routbort, T.O. Mason, J. Appl. Phys. 87 (2000) 117.
[4] S. Schumann, R. Da Campo, B. Illy, A.C. Cruickshank, M.A. McLachlan, M.P. Ryan, D.J. Riley, D.W. McComb, T.S. Jones, J. Mater. Chem. 21 (2011) 2381.
[5] J. Boucle, P. Ravirajan, J. Nelson, J. Mater. Chem. 17 (2007) 3141.
[6] T. Yang, W. Cai, D. Qin, E. Wang, L. Lan, X. Gong, J. Peng, Y. Cao, J. Phys. Chem. C. 114 (2010) 6849.
[7] S. Kasap, J.B. Frey, G. Belev, O. Tousignant, H. Mani, J. Greenspan, L. Laperriere, O. Bubon, A. Reznik, G. DeCrescenzo, K.S. Karim, J.A. Rowlands, Sensors 11 (2011) 5112.
[8] A.R. Cowen, S.M. Kengyelics, A.G. Davies, Clin. Radiol. 63 (2008) 487.
[9] J.A. Seibert, Pediatr. Radiol. 36 (2006) 173.
[10] A. Reznik, S.D. Baranovskii, O. Rubel, G. Juska, S.O. Kasap, Y. Ohkawa, K. Tanioka, J.A. Rowlands, J. Appl. Phys. 102 (2007) 053711.
[11] O. Rubel, A. Potvin, D. Laughton, J. Phys.-Condes. Matter 23 (2011) 055802.
[12] M.M. Wronski, W. Zhao, A. Reznik, K. Tanioka, G. DeCrescenzo, J.A. Rowlands, Med. Phys. 37 (2010) 4982.
[13] K. Tanioka, J. Mater. Sci.-Mater. Electron 18 (2007) 321.
[14] G. Belev, S.O. Kasap, J. Non-Cryst. Solids 352 (2006) 1616.
[15] J.B. Frey, G. Belev, O. Tousignant, H. Mani, S.O. Kasap, Phys. status solidi C. 6 (2009) S251.
[16] S.A. Mahmood, M.Z. Kabir, O. Tousignant, H. Mani, J. Greenspan, P. Botka, Appl. Phys. Lett. 92 (2008) 223506.
[17] S. Kasap, J.B. Frey, G. Belev, O. Tousignant, H. Mani, L. Laperriere, A. Reznik, J.A. Rowlands, Phys. status solidi B 246 (2009) 1794.
[18] S. Kasap, G. Belev, J. Optoelectron. Adv. Mater. 9 (2007) 1.
[19] K. Sugiyama, H. Ishii, Y. Ouchi, K. Seki, J. Appl. Phys. 87 (2000) 295.
[20] Z. Guo, D. Zhao, Y. Liu, D. Shen, J. Zhang, B. Li, Appl. Phys. Lett. 93 (2008) 163501.
[21] C.H. Ahn, Y.Y. Kim, D.C. Kim, S.K. Mohanta, H.K. Cho, J. Appl. Phys. 105 (2009) 013502.
[22] Q.P. Wang, D.H. Zhang, Z.Y. Xue, X.J. Zhang, Opt. Mater. 26 (2004) 23.
[23] O. Bubon, G. DeCrescenzo, J.A. Rowlands, A. Reznik, J. Non-Cryst. Solids 358 (2012) 2431.
[24] A. Sultana, M.M. Wronski, K.S. Karim, J.A. Rowlands, IEEE Sens. J. 10 (2010) 347.
[25] P.T. Hsieh, Y.C. Chen, C.M. Wang, Y.Z. Tsai, C.C. Hu, Appl. Phys. A-Mater. Sci. Process 84 (2006) 345.
[26] P.T. Hsieh, Y.C. Chen, K.S. Kao, C.M. Wang, Appl. Phys. A-Mater. Sci. Process 90 (2008) 317.
[27] X.Q. Wei, B.Y. Man, M. Liu, C.S. Xue, H.Z. Zhuang, C. Yang, Phys. B 388 (2007) 145.
[28] Z.G. Wang, X.T. Zu, S. Zhu, L.M. Wang, Phys. E 35 (2006) 199.
[29] T.G.G. Maffeis, M.W. Penny, A. Castaing, O.J. Guy, S.P. Wilks, Surf. Sci. 606 (2012) 99.
[30] M. Li, G. Xing, L.F.N. Ah Qune, G. Xing, T. Wu, C.H.A. Huan, X. Zhang, T.C. Sum, Phys. Chem. Chem. Phys. 14 (2012) 3075.
[31] N. Ashkenov, B.N. Mbenkum, C. Bundesmann, V. Riede, M. Lorenz, D. Spemann, E.M. Kaidashev, A. Kasic, M. Schubert, M. Grundmann, G. Wagner, H. Neumann, V. Darakchieva, H. Arwin, B. Monemar, J. Appl. Phys. 93 (2003) 126.
[32] C. Chandrinou, N. Boukos, C. Stogios, A. Travlos, Microelectron. J. 40 (2009) 296.
[33] I.C. Yao, T.-Y. Tseng, P. Lin, Sens. Actuator A-Phys. 178 (2012) 26.
[34] B. Lin, Z. Fu, Y. Jia, Appl. Phys. Lett. 79 (2001) 943.
[35] K. Vanheusden, W.L. Warren, C.H. Seager, D.R. Tallant, J.A. Voigt, B.E. Gnade, J. Appl. Phys. 79 (1996) 7983.
[36] B. Cao, W. Cai, H. Zeng, Appl. Phys. Lett. 88 (2006) 161101.
[37] L.S. Vlasenko, G.D. Watkins, Phys. Rev. B 71 (2005) 125210.
[38] X. Meng, Z. Shi, X. Chen, X. Zeng, F. Zhuxi, J. Appl. Phys. 107 (2010) 023501.
[39] G. Xiong, U. Pal, J.G. Serrano, J. Appl. Phys. 101 (2007) 024317.
[40] Y.-P. Wang, W.-I. Lee, T.-Y. Tseng, Appl. Phys. Lett. 69 (1996) 1807.
[41] A.Y. Polyakov, N.B. Smirnov, A.V. Govorkov, E.A. Kozhukhova, V.I. Vdovin, K. Ip, M.E. Overberg, Y.W. Heo, D.P. Norton, S.J. Pearton, J.M. Zavada, V.A. Dravin, J. Appl. Phys. 94 (2003) 2895.
[42] Z.-Q. Fang, B. Claflin, D.C. Look, L.L. Kerr, X. Li, J. Appl. Phys. 102 (2007) 023714.
[43] F. Oba, A. Togo, I. Tanaka, J. Paier, G. Kresse, Phys. Rev. B 77 (2008) 245202.
[44] S. Lany, A. Zunger, Phys. Rev. B 72 (2005) 035215.
[45] S.B. Zhang, S.H. Wei, A. Zunger, Phys. Rev. B 63 (2001) 075205.
[46] T.R. Paudel, W.R.L. Lambrecht, Phys. Rev. B 77 (2008) 205202.
[47] K. Kikuchi, Y. Ohkawa, K. Miyakawa, T. Matsubara, K. Tanioka, M. Kubota, N. Egami, Phys. status solidi C. 8 (2011) 2800.
[48] S. Abbaszadeh, N. Allec, S. Ghanbarzadeh, U. Shafique, K.S. Karim, IEEE Trans. Electron Devices 59 (2012) 2403.